

Neat, Simple, and Wrong: Debunking Electrostatic Fallacies Regarding Noncovalent Interactions

John M. Herbert*



Cite This: *J. Phys. Chem. A* 2021, 125, 7125–7137



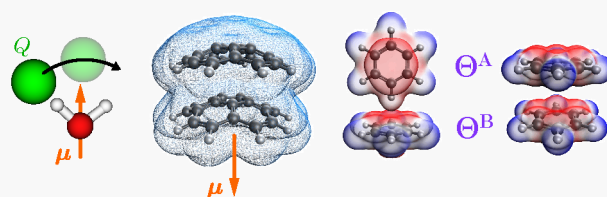
Read Online

ACCESS |

Metrics & More

Article Recommendations

ABSTRACT: Multipole moments such as charge, dipole, and quadrupole are often invoked to rationalize intermolecular phenomena, but a low-order multipole expansion is rarely a valid description of electrostatics at the length scales that characterize nonbonded interactions. This is illustrated by examining several common misunderstandings rooted in erroneous electrostatic arguments. First, the notion that steric repulsion originates in Coulomb interactions is easily disproved by dissecting the interaction potential for Ar₂. Second, the Hunter-Sanders model of π–π interactions, which is based on quadrupolar electrostatics, is shown to have no basis in accurate calculations. Third, curved “buckybowls” exhibit unusually large dipole moments, but these are ancillary to the forces that control their intermolecular interactions, as illustrated by two examples involving corannulene. Finally, the assumption that interactions between water and small anions are dictated by the dipole moment of H₂O is shown to be false in the case of binary halide–water complexes. These examples present a compelling case that electrostatic explanations based on low-order multipole moments are very often counterfactual for nonbonded interactions at close range and should not be taken seriously in the absence of additional justification.



$$\varphi(\mathbf{R}) = \frac{Q}{R} + \frac{\boldsymbol{\mu} \cdot \mathbf{R}}{R^3} + \frac{\mathbf{R}^\dagger \mathbf{Q} \mathbf{R}}{R^5} + \dots$$

1. PHILOSOPHY

Chemistry has sometimes been called the “central science”,^{1–3} which is perhaps appropriate for a discipline that is situated somewhere between the reductionism of physics and the emergent complexity of biology.^{3,4} On the biological end of that spectrum there is no shame in arguments based on a careful, empirical categorization of observed phenomena (or what Ernest Rutherford famously derided as mere “stamp collecting”),⁵ precisely because emergent complexity suggests that it is a fallacy of reductionist epistemology to believe that the laws of one discipline can be viewed as trivial consequences of the laws of another discipline.^{6,7}

Reductionism survives in (physical) chemistry, yet so does complexity. Crucially, the entire chemical enterprise is largely contained within a narrow free energy window measured in tens of kilocalories per mole. Chemical phenomena are often balanced on a knife-edge of near-cancellation of attractive and repulsive forces, leading to an energetic driving force that is tiny in comparison to various competing interactions. Subtleties abound. Oft-quoted examples include the dipole moment of the carbon monoxide molecule (C^{δ−}–O^{δ+}), which points in the “wrong” direction,^{8,9} and the fact that the electron affinity of chlorine atom is slightly larger than that of fluorine,¹⁰ in stubborn defiance of a periodic trend.¹¹

This complexity should not deter us from seeking the simplest (correct) explanations for chemical phenomena. A practical

definition of a physical chemist, which encompasses both theory and experiment, might be someone who seeks to construct and interrogate *models* of complex chemical phenomena, with the idea that those models might more easily yield to detailed understanding. Such models then form a framework through which we rationalize the behavior of more complicated systems. Physics-inspired reductionism, however, should always respect *Einstein’s razor*: that things should be made as simple as possible, but not simpler.

In this author’s experience, the study of noncovalent interactions is an area ripe with examples where reductionism has been pushed beyond its breaking point, sacrificing correctness at the alter of simplicity. This Perspective is constructed around several such examples, for which incorrect rationalizations based on low-order multipole moments stubbornly persist in textbooks and in pedagogy. A recurring theme is that explanations based on molecular multipole moments, which are defined via asymptotic expansion of the

Received: July 4, 2021

Revised: July 30, 2021

Published: August 13, 2021



molecular electrostatic potential, are almost never justified at the intermolecular separations that characterize nonbonded close-contact interactions.

Section 2 of this work introduces a tool by means of which these phenomena can be understood on a rigorous footing, while Section 3 explores a sequence of “electrostatic myths”: explanations that are widespread but do not stand up to close scrutiny. Section 4 discusses a possible solution to this conundrum in the form of distributed multipoles, an old idea but one that ought to be taken more seriously in chemical pedagogy.

2. ENERGY DECOMPOSITION

The focus of this Perspective is on qualitative explanations, but each example is backed by quantitative calculations, based on the formalism of symmetry-adapted perturbation theory (SAPT).^{12–18} Briefly, SAPT modifies the long-range perturbation theory of intermolecular interactions^{18–22} in order to satisfy the antisymmetry requirement at short range. It also provides a decomposition of the intermolecular interaction energy (E_{int}) into physically meaningful components,^{23,24}

$$E_{\text{int}}^{\text{SAPT}} = E_{\text{elst}} + E_{\text{exch}} + E_{\text{ind}} + E_{\text{disp}} \quad (1)$$

The terms in this expression represent electrostatics (E_{elst}), Pauli or “exchange” repulsion (E_{exch}), induction (E_{ind}), and dispersion (E_{disp}).^{22–24} Each of these components is briefly explained below; see refs 18 and 22 for additional elaboration.

2.1. Electrostatics. The E_{elst} term in eq 1 is the main focus of the present work and is singled out for a detailed elaboration. This component of the interaction energy is essentially classical but is computed using quantum-mechanical electron densities, from a Hartree–Fock calculation for example (in the simplest version of the theory). It can be separated into internuclear repulsion ($E_{\text{elst}}^{\text{nn}} > 0$), electron–electron repulsion ($E_{\text{elst}}^{\text{ee}} > 0$), and electron–nuclear attraction ($E_{\text{elst}}^{\text{en}} < 0$) contributions:²³

$$E_{\text{elst}} = E_{\text{elst}}^{\text{nn}} + E_{\text{elst}}^{\text{ee}} + E_{\text{elst}}^{\text{en}} \quad (2)$$

For a noncovalent complex A...B with isolated-monomer electron densities $\rho_0^{\text{A}}(\mathbf{r})$ and $\rho_0^{\text{B}}(\mathbf{r})$, these three components are defined as

$$E_{\text{elst}}^{\text{nn}} = \sum_{a \in \text{A}} \sum_{b \in \text{B}} \frac{Z_a Z_b}{R_{ab}} \quad (3a)$$

$$E_{\text{elst}}^{\text{ee}} = \int \frac{\rho_0^{\text{A}}(\mathbf{r}_1) \rho_0^{\text{B}}(\mathbf{r}_2)}{\|\mathbf{r}_1 - \mathbf{r}_2\|} d\mathbf{r}_1 d\mathbf{r}_2 \quad (3b)$$

$$E_{\text{elst}}^{\text{en}} = - \sum_{a \in \text{A}} \int \frac{Z_a \rho_0^{\text{B}}(\mathbf{r})}{\|\mathbf{r} - \mathbf{R}_a\|} d\mathbf{r} - \sum_{b \in \text{B}} \int \frac{Z_b \rho_0^{\text{A}}(\mathbf{r})}{\|\mathbf{r} - \mathbf{R}_b\|} d\mathbf{r} \quad (3c)$$

for atomic numbers Z_a and Z_b . (These and subsequent equations are expressed in atomic units, where $e^2/4\pi\epsilon_0 = 1$.) The signs in eq 3c reflect the convention that electron densities are output from electronic structure programs as strictly positive quantities, representing probability densities of negatively charged electrons.

Electrostatic interactions can alternatively be expressed in terms of electrostatic potentials. For isolated monomer A, considering the contributions from both electrons and nuclei, the electrostatic potential is

$$\varphi_0^{\text{A}}(\mathbf{R}) = - \int \frac{\rho_0^{\text{A}}(\mathbf{r})}{\|\mathbf{r} - \mathbf{R}\|} d\mathbf{r} + \sum_{a \in \text{A}} \frac{Z_a}{\|\mathbf{R} - \mathbf{R}_a\|} \quad (4)$$

To proceed, let us introduce a composite charge density $\tilde{\rho}_0^{\text{B}}(\mathbf{r})$ for isolated monomer B, which contains both electrons and nuclei:

$$\tilde{\rho}_0^{\text{B}}(\mathbf{r}) = -\rho_0^{\text{B}}(\mathbf{r}) + \sum_{b \in \text{B}} Z_b \delta(\mathbf{r} - \mathbf{R}_b) \quad (5)$$

The total electrostatic interaction in eq 2 can be expressed succinctly in terms of the electrostatic potential for A and the total charge density for B:

$$E_{\text{elst}} = \int \varphi_0^{\text{A}}(\mathbf{r}) \tilde{\rho}_0^{\text{B}}(\mathbf{r}) d\mathbf{r} \quad (6)$$

SAPT electrostatics calculations evaluate the integrals in eqs 3b and 3c analytically, using the basis-set representations of the monomer densities, and the electrostatic potential is not required. However, color-coded maps of $\varphi_0^{\text{A}}(\mathbf{r})$ are a common qualitative analysis tool and are available from many electronic structure programs. More to the point, we have introduced the electrostatic potential in order to introduce its multipolar expansion,^{20,21,25,26} which is

$$\varphi_0^{\text{A}}(\mathbf{R}) = \frac{Q^{\text{A}}}{R} + \frac{\boldsymbol{\mu}^{\text{A}} \cdot \mathbf{R}}{R^3} + \frac{\mathbf{R}^{\dagger} \boldsymbol{\Theta}^{\text{A}} \mathbf{R}}{R^5} + \dots \quad (7)$$

The charge Q^{A} , dipole moment vector $\boldsymbol{\mu}^{\text{A}}$, quadrupole moment tensor $\boldsymbol{\Theta}^{\text{A}}$, etc., are the multipole moments of a charge density $\tilde{\rho}_0^{\text{A}}$ that is defined similarly to eq 5. This is the form in which molecular multipole moments are typically output by electronic structure programs. For example, $Q^{\text{A}} = 0$ for a charge-neutral molecule, which can only be the case if the moments in eq 7 correspond to the total charge density $\tilde{\rho}_0^{\text{A}}$, including both nuclei and electrons, and not just the electron density ρ_0^{A} .

The charge density $\tilde{\rho}_0^{\text{B}}(\mathbf{r})$ that appears in eq 6 has its own multipole expansion, analogous to eq 7, and the lowest nonvanishing multipolar interaction term between A and B dictates the long-range behavior of E_{elst} . Although it is sometimes assumed that the multipole expansion is exact if taken to all orders (even if it is invariably truncated in practice), in fact this expansion is known to be divergent at a short range.^{18,20,26,27} At a minimum, any low-order multipolar approximation to E_{elst} is likely invalid once the electron clouds of A and B begin to interpenetrate. This has been called the “charge penetration effect”.^{17,18,27–30}

2.2. Other Energy Components. Having rigorously introduced the electrostatic component of E_{int} , the remaining energy components in eq 1 will be summarized more briefly.

For reasons of formal and computational simplicity, the unperturbed reference state for SAPT is a direct product $|\psi_0^{\text{A}} \psi_0^{\text{B}}\rangle$ rather than an antisymmetrized product.³¹ The exchange interaction (E_{exch} in eq 1) is the leading-order correction for $\text{A} \leftrightarrow \text{B}$ antisymmetry.²³ It is repulsive, because the wave functions ψ_0^{A} and ψ_0^{B} are computed in isolation, so there is an energetic penalty to deform them into compliance with the Pauli exclusion principle, or equivalently, a penalty to orthogonalize the molecular orbitals (MOs) on A with respect to those on B.³² For this reason, E_{exch} can equivalently be called *Pauli repulsion*.

The induction energy E_{ind} arises at the second order in perturbation theory²⁴ and includes what is commonly understood as *polarization*, namely, deformation of monomer A’s electron cloud in the presence of monomer B and *vice versa*. Less

obviously, E_{ind} also includes intermolecular charge transfer (CT):

$$E_{\text{ind}} = E_{\text{pol}} + E_{\text{CT}} \quad (8)$$

There are various means to separate these two components,^{33–36} but that discussion is deferred for now. (Of the systems considered here, only the anion–water complexes in Section 3.4 exhibit significant induction energies.)

Finally, the dispersion energy E_{disp} arises from correlated, quantum-mechanical fluctuations in the density, as first explained by London.^{37–40} (The term “dispersion” is an analogy to the fact that the quantum-mechanical theory bears similarities to that of optical dispersion.^{37–39}) These forces are responsible for the observation, made much earlier by van der Waals,⁴¹ that all matter is attractive at a sufficiently long range. The “fluctuations” that are required occur with respect to the mean-field Hartree–Fock reference state, $|\Psi_0\rangle = |\psi_0^A \psi_0^B\rangle$. In a configuration interaction expansion of the exact wave function, matrix elements $\langle \Psi_0 | \hat{H} | \Psi_{ij}^{ab} \rangle$ involving double excitations generate long-range attraction even in cases where the individual monomers have no dipole moments. (London also demonstrated that the quadrupole moments of H_2 and N_2 are insufficient to explain the magnitude of the deviations from ideal-gas behavior,³⁷ thus dispelling an alternative hypothesis for the origin of long-range attraction.) Double excitations appear at second order in perturbation theory and therefore the leading-order formula for dispersion is

$$E_{\text{disp}}^{(2)} = - \sum_{m>0} \sum_{n>0} \frac{|\langle \psi_m^A \psi_n^B | \hat{V} | \psi_0^A \psi_0^B \rangle|^2}{(\epsilon_n^A - \epsilon_0^A)(\epsilon_n^B - \epsilon_0^B)} \quad (9)$$

where $\hat{V} = \hat{H}_{\text{AB}} - \hat{H}_{\text{A}} - \hat{H}_{\text{B}}$.^{19,22} The matrix element in the numerator of eq 9 can be interpreted as the electrostatic interaction between transition densities $\rho_{m0}^A(\mathbf{r})$ and $\rho_{n0}^B(\mathbf{r})$,^{19,20} so that dipole–dipole (and higher-order multipolar) interactions appear even if the unperturbed densities $\rho_0^A(\mathbf{r})$ and $\rho_0^B(\mathbf{r})$ are spherically symmetric.

Dispersion interactions, or noncovalent interactions more generally, are often called “van der Waals” (vdW) interactions, but this terminology is imprecise. In the eponymous vdW equation of state for nonideal gases,⁴¹ attractive and repulsive interactions are introduced as separate, empirical corrections to a noninteracting model. Similarly, E_{disp} and E_{exch} are separate energy components with very different origins, one of which reflects a general cohesive interaction and the other embodies finite molecular size. The sum of these components,

$$\begin{aligned} E_{\text{vdW}} &= E_{\text{exch}} + E_{\text{disp}} \\ &= E_{\text{int}} - E_{\text{elst}} - E_{\text{ind}} \end{aligned} \quad (10)$$

might sensibly be called the vdW interaction, in homage to its namesake.^{30,42} Pauli repulsion and dispersion compete in interesting and sometimes counterintuitive ways, as bulky substituents such as *tert*-butyl contribute significantly to both E_{exch} and E_{disp} .⁴³ Whereas these two energy components are quantum-mechanical in origin, the remaining components have a quasiclassical interpretation and

$$E_{\text{elst+ind}} = E_{\text{elst}} + E_{\text{ind}} \quad (11)$$

will be called *polarized electrostatics*.

2.3. Overview of Methods. The formalism outlined above can be regarded as a form of energy decomposition analysis (EDA),^{44–46} albeit a rather special one with considerably less

arbitrariness as compared to EDAs that are based on supramolecular density functional theory (DFT).⁴⁶ The latter approaches are take-it-or-leave-it affairs, wherein the quality of the energy components is beholden to the quality of the density-functional approximation. Historically, the description of nonbonded interactions in DFT has been rather uneven, with dispersion interactions being particularly problematic.⁴⁷ This situation is significantly improved in contemporary DFT by means of empirical dispersion corrections,^{47,48} but separability remains a problem and these “+D” corrections to DFT should not be interpreted as a true dispersion.^{35,38,49–51}

Supramolecular calculation of the A···B interaction energy,

$$E_{\text{int}}^{A\cdots B} = E^{AB} - E^A - E^B \quad (12)$$

is also afflicted by basis set superposition error (BSSE).⁵² This is an artifact of atom-centered basis sets and presents a quandary for many EDAs, whereas BSSE is absent in SAPT calculations because E_{int} is computed directly from perturbation theory and not by subtraction. As an example of the effects of BSSE, interaction potentials $E_{\text{int}}(R)$ for Ar_2 are plotted in Figure 1,

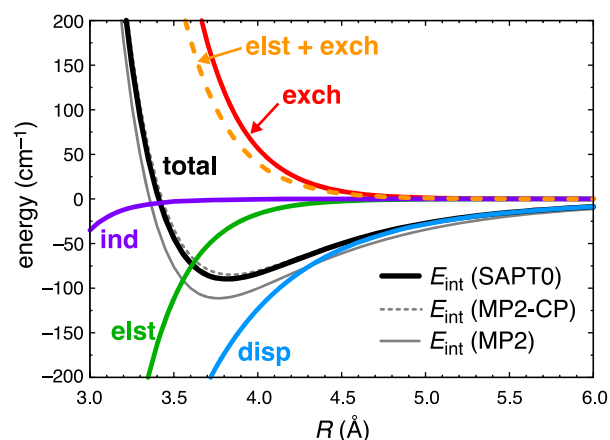


Figure 1. Total interaction potential $E_{\text{int}}(R)$ for Ar_2 (in black) and its SAPT decomposition (in color), computed at the SAPT0/aug-cc-pVTZ level. The two curves in gray represent $E_{\text{int}}(R)$ computed at the MP2/aug-cc-pVTZ level, either with counterpoise correction (MP2-CP, dashed curve) or without (solid curve).

computed at the level of second-order Møller–Plesset perturbation theory (MP2). With counterpoise correction for BSSE,⁵² the MP2 potential is in good agreement the second-order “SAPT0” method,⁵³ but in the absence of the counterpoise correction the MP2 interaction energy is 30% larger at the equilibrium separation.

In contrast to the supramolecular approach, the quality of the approximation is improvable in SAPT, by going to higher orders in perturbation theory,^{12,53} for example, and can be pushed to the *ab initio* limit.^{53,54} The dispersion term is the most challenging, but the inherent separability of the SAPT interaction energy can be used to replace second-order dispersion with a more accurate alternative.^{16,55–61} A variety of SAPT methods is used in the examples presented below, perhaps most notably the XSAPT + MBD approach,^{16,59–61} which includes many-body dispersion (MBD) and is based upon an “extended” (X)SAPT formalism.^{57–59,62} Among low-cost electronic structure methods, XSAPT + MBD is one of the most accurate methods for noncovalent interaction energies,

achieving mean errors < 1 kcal/mol in various benchmark tests.^{16,60,61}

3. DEBUNKING ELECTROSTATIC MYTHS

The main part of this work explores several “just-so stories”, in which electrostatic arguments seem to provide a straightforward explanation for an observed phenomenon yet fail to withstand detailed scrutiny. Each section below is organized around a certain “electrostatic myth” that the present work aims to discredit.

3.1. Myth: Steric Repulsion is Coulomb Repulsion. The connection between the Pauli exclusion principle and steric repulsion has been understood for a long time,⁶³ yet the fallacy that steric repulsion is primarily driven by electron–electron Coulomb repulsion continues to pervade chemical education. Consider Ar_2 as a simple example, whose interaction energy profile $E_{\text{int}}(R)$ is shown in Figure 1 along with its SAPT decomposition. It is immediately clear that Pauli repulsion (E_{exch}), rather than electrostatics, is what furnishes the repulsive part of the potential, as $E_{\text{elst}}(R)$ remains attractive well inside of the minimum-energy $\text{Ar}\cdots\text{Ar}$ separation. This implies that the dominant electrostatic effect is not electron–electron repulsion but rather the fact that electrons on one monomer gain access to the nucleus on the other. This may seem counterintuitive, and in fact the effect is quite subtle as the attractive and repulsive parts of E_{elst} are nearly balanced. Examining the minimum-energy Ar_2 separation, for example, and using the level of theory that is reported in Figure 1, one obtains $E_{\text{elst}}^{\text{nn}} = +45.119\ 320$ Ha, $E_{\text{elst}}^{\text{ee}} = +45.119\ 419$ Ha, and $E_{\text{elst}}^{\text{en}} = -90.238\ 903$ Ha (in Hartree atomic units). The sum of these is $E_{\text{elst}} = -0.000\ 164$ Ha = -35.9 cm⁻¹, which is the value plotted in Figure 1 at $R = 3.8$ Å.

From a certain point of view, $E_{\text{elst}} + E_{\text{exch}}$ might best be considered together because it is their sum that approximates the electrostatic interaction of an antisymmetrized reference state. On the one hand, this sum indeed gives rise to a repulsive potential (see Figure 1). On the other hand, from the standpoint of classical modeling, it is the generally the isolated-monomer charge density that is subjected to a multipole expansion. From that perspective, the non-antisymmetrized SAPT definition of electrostatics (consisting of E_{elst} alone) is the appropriate one.

This example provides an important lesson, namely, that electrostatic interactions between isolated-monomer densities can be attractive at length scales characteristic of vdW complexes, even in cases where there is no long-range electrostatic attraction. The next example demonstrates that short-range electrostatics can be attractive even in cases where the long-range electrostatic interaction is repulsive.

3.2. Myth: Quadrupolar Electrostatics Drives π – π Interactions. There is perhaps no better example of the misuse of low-order multipole moments than the analysis of benzene dimer's stereoisomers in terms of the quadrupole moment of C_6H_6 . Introduced by Hunter and Sanders in 1990,⁶⁴ this paradigm has since made its way into textbooks as a general explanation of arene–arene conformational preferences.^{65,66} It posits that the electron-withdrawing or electron-donating character of an aryl substituent modulates π -stacking energies via its effect on the quadrupole moment of the aromatic moiety. However, modern *ab initio* calculations do not support this picture,^{28,67–74} which has also been questioned on the basis of stacking energies obtained from measurements of conformational equilibria.^{75–77} Although alternative explanations for π – π substituent effects have emerged,^{69–74} the Hunter-Sanders picture continues to be invoked in recent literature.^{78–83}

The kernel of truth at the origin of the Hunter-Sanders myth is an experimental measurement of the C_6H_6 quadrupole mo-

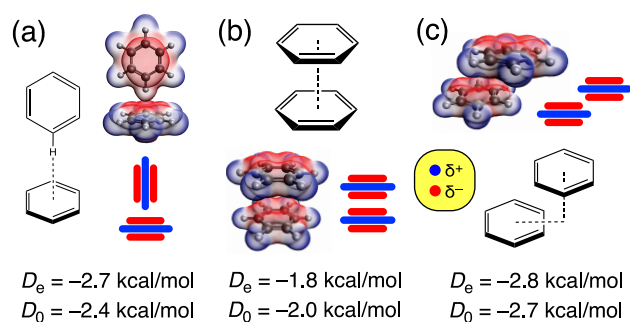


Figure 2. Stereoisomers of benzene dimer: (a) T-shaped geometry, (b) eclipsed-cofacial geometry, and (c) parallel-displaced or offset-stacked geometry. Benchmark interaction energies for the gas-phase dimer are indicated.⁸⁵ Also shown are electrostatic potential maps and cartoon representations of the monomer charge distributions.

ment,⁸⁴ whose sign corresponds to electropositive C–H bonds sandwiched between π -electron densities. This is depicted schematically in Figure 2, which also shows the canonical stereoisomers of $(\text{C}_6\text{H}_6)_2$. Benchmark-quality *ab initio* calculations^{68,85} suggest that the T-shaped C–H $\cdots\pi$ isomer (Figure 2a) lies within 1 kcal/mol of the eclipsed-cofacial isomer (Figure 2b), which is an energetic saddle point connecting parallel-displaced structures (Figure 2c) that are slightly lower in energy. The Hunter-Sanders model, based either qualitatively on the charge distributions suggested in Figure 2 or quantitatively on the quadrupole moments of the monomers, posits that the relative energies of these isomers emerge from a competition between dispersion and quadrupolar electrostatics. Dispersion is nonspecific as to angular orientation but favors atomic close-contacts, due to its R^{-6} falloff with distance, and is most favorable in the cofacial arrangement. As suggested by the charge distributions in Figure 2, however, the quadrupole–quadrupole interaction is repulsive in parallel (cofacial) arrangements but attractive in perpendicular (T-shaped) configurations. The fact that other aromatic molecules also exhibit offset stacking in their crystal structures is taken as evidence for the generality of this picture.⁶⁵ A survey by Hunter et al.⁸⁶ of spatially proximate phenylalanine side chains in protein crystal structures reveals that these are arranged in either T-shaped or offset-stacked geometries and are rarely found in cofacial orientations. The leap from $(\text{C}_6\text{H}_6)_2$ to proteins is left to the reader.

One ought to be suspicious of arguments about short-range interactions that are based on low-order multipole moments, and a comparison of exact versus multipolar electrostatics for benzene dimer (Figure 3) confirms these suspicions.²⁹ The multipole approximation for E_{elst} represented in Figure 3 using quadrupole and octupole moments, is asymptotically correct, but this asymptote is recovered only for intermolecular separations $\gtrsim 4.0$ – 4.5 Å, as compared to the 3.8 Å face-to-face distance in the eclipsed-cofacial geometry and the 3.4 Å separation in the parallel-displaced configuration. In the 3.4–3.8 Å range, exact electrostatics is attractive for both parallel and perpendicular arrangements of benzene dimer.

To understand the true origin of conformational preferences in $(\text{C}_6\text{H}_6)_2$, we consider energy components along a “sliding coordinate”, for both parallel and perpendicular arrangements of the dimer.⁴² Plotted in Figure 4 is the polarized electrostatics energy ($E_{\text{elst+ind}}$) along this coordinate, although E_{ind} is quite

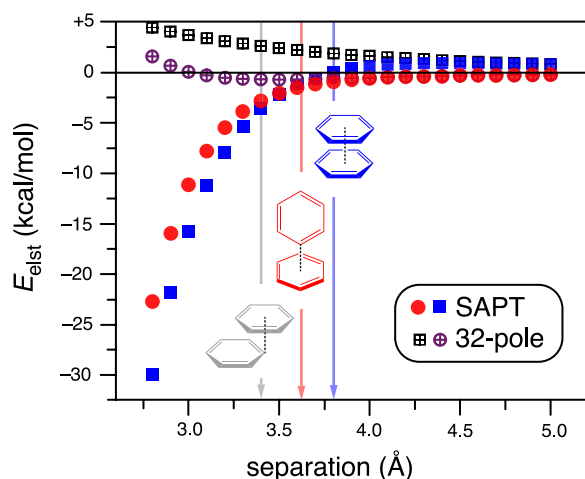


Figure 3. Electrostatic interaction energies for the cofacial (blue) and T-shaped (red) isomers of $(C_6H_6)_2$, as a function of intermolecular distance. Solid symbols indicate E_{elst} from a SAPT0+ δE_{HF} /jun-cc-pVDZ calculation, whereas open symbols with crosses correspond to a multipole potential including both quadrupole–quadrupole and octupole–quadrupole terms. Arrows indicate the intermolecular separations for the various isomers that are shown. Adapted from ref 29, copyright 2016 American Chemical Society.

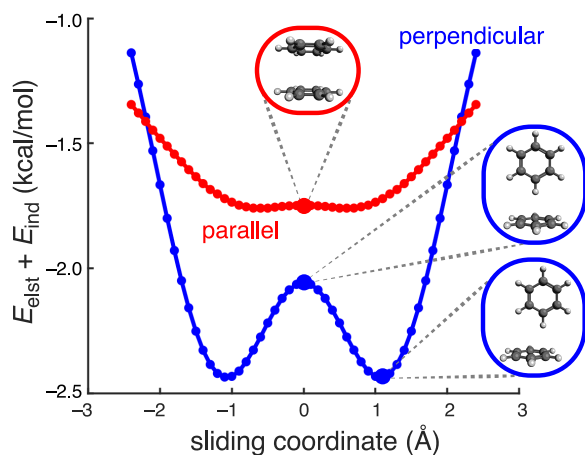


Figure 4. Polarized electrostatics ($E_{\text{elst+ind}}$) energy profiles along a coordinate where one benzene monomer slides past another in either a cofacial or a perpendicular orientation. The face-to-face separation in the parallel arrangement is 3.8 Å, consistent with the cofacial saddle point in Figure 2b, whereas the center-to-center distance in the perpendicular arrangement is 5.0 Å at zero displacement, consistent with the T-shaped structure in Figure 2a. Energies were computed using the XSAPT+MBD approach.⁶⁰ Adapted from ref 42 under a CC BY 3.0 license.

small, so this is mostly a plot of how E_{elst} changes upon slip-stacking (in the parallel orientation) or else upon T-shaped to L-shaped displacement (in the perpendicular arrangement). For the cofacial isomer, E_{elst} hardly changes at all, and parallel displacements of ± 1 Å incur essentially zero electrostatic penalty. Larger displacements, which the Hunter-Sanders model asserts should be driven by a reduction in quadrupolar electrostatics, actually cause $E_{\text{elst+ind}}$ to become less attractive. In reality, neither electrostatics nor polarization provides a driving force for offset-stacking.

By a process of elimination, the remaining energy components (Pauli repulsion and dispersion) must explain why the parallel-

displaced arrangement is lower in energy. This “vdW potential” (eq 10) is plotted in Figure 5 along with the total interaction potential, for both parallel and perpendicular configurations of $(C_6H_6)_2$. In both cases, E_{vdW} exhibits the same conformational preferences as E_{int} , namely, a T-shaped geometry (rather than an L-shaped one) when the monomers are constrained to be perpendicular and an offset of a bit more than half the ring size when the monomers are in a parallel orientation.

The vdW potential evidently furnishes the driving force for offset stacking. Dispersion is enhanced by maximization of the cofacial area and favors the eclipsed-cofacial geometry; however, the electron densities $\rho_0^A(\mathbf{r})$ and $\rho_0^B(\mathbf{r})$ have cusps at the nuclei and the eclipsed-cofacial arrangement aligns these cusps atop one another. This incurs a Pauli repulsion penalty that is relieved by offset stacking. (Rotation of one monomer about its C_6 symmetry axis lowers the energy by less than 0.1 kcal/mol, because the density maxima remain nearly coincident.)

It is worth noting that the energy scales in Figures 4 and 5 span a range of <4 kcal/mol. It is therefore crucial that the theoretical method used to draw these conclusions (XSAPT+MBD) exhibits an accuracy better than 1 kcal/mol when applied to benchmark small-molecule data sets.^{59–61} The nature of dispersion in DFT makes it difficult to separate this energy component from the others,^{49–51} even for functionals that perform well for nonbonded interactions (and many functionals do not). As such, it would be difficult to make a convincing case about the driving forces for π -stacking on the basis of supramolecular DFT calculations alone.

Whereas Hunter and Sanders used point charges, in conjunction with atom–atom dispersion and repulsion potentials, to describe the conformational preferences of benzene dimer,⁶⁴ an equally simple model omits electrostatics and pairs the dispersion potential with a Gaussian overlap model of Pauli repulsion. This vdW model (dispersion + Pauli repulsion) successfully describes the conformational preferences of a benzene dimer⁴² and larger acene dimers,³⁰ without appeal to electrostatics. It can explain the fact that small aromatic molecules exhibit offset stacking on the surface of graphene,^{30,87} where the quadrupolar interactions have saturated as a function of size and for which the Hunter-Sanders model fails qualitatively.¹⁶

The vdW model does not rely on quadrupole moments and therefore offers a convincing explanation for why the $(C_6H_6)\cdots(C_6F_6)$ heterodimer exhibits a minimum-energy geometry that is parallel-displaced.^{88–90} The original Hunter-Sanders work did not consider this system, which is an interesting omission given that quadrupole moments for both benzene and hexafluorobenzene were reported in the same experimental paper:⁸⁴ $\Theta(C_6H_6) = -8.69 \pm 0.51$ B and $\Theta(C_6F_6) = +9.50 \pm 0.51$ B, similar in magnitude but opposite in sign.⁹¹ The ramification of the sign change is that dispersion and quadrupolar electrostatics no longer compete in $(C_6H_6)\cdots(C_6F_6)$, but instead both forces favor cofacial stacking. Nevertheless, the parallel-displaced isomer is slightly lower in energy, by 0.3 kcal/mol as compared to the eclipsed-cofacial isomer.⁸⁹

The observation of offset stacking in $(C_6H_6)\cdots(C_6F_6)$ is easy to rationalize within the vdW model because perfect cofacial stacking still incurs a Pauli repulsion penalty, independent of the sign of the quadrupole moment. This explanation is borne out by SAPT calculations.⁴² More speculatively, the vdW model might better explain the prevalence of offset stacking (and the near-absence of cofacial stacking) in protein crystal structures,⁸⁶ where the data set presumably samples many different local

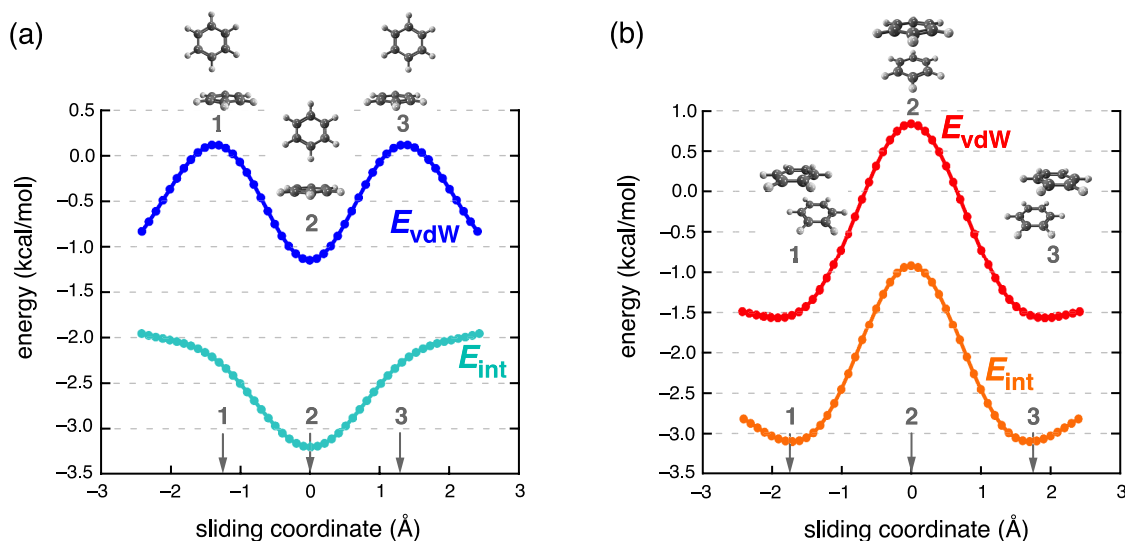


Figure 5. Total interaction potentials (E_{int}) vs vdW potentials (E_{vdW} , eq 10) for sliding one benzene monomer past another in either (a) the perpendicular orientation or (b) the parallel orientation. Arrows at the bottom of each panel indicate the position coordinate of the structures that are shown. Energies were computed using the XSAPT+MBD approach.⁶⁰ Adapted from ref 42 under a CC BY 3.0 license.

electrostatic environments, yet offset-stacking persists. According to the vdW model, this is because the forces responsible (dispersion and Pauli repulsion) are inherently short-ranged.

The fact that electrostatics is not required to obtain offset stacking does not imply that electrostatics is uniformly unimportant in π -stacking situations. The most convincing explanation for substituent effects on stacking energies, for example, is the “direct interaction model” introduced by Wheeler and Houk,^{69–73} in which the most important effect is how the local dipole moment of a substituent moiety on one aromatic ring interacts with the electric field of its π -stacked partner.⁷³ This picture is supported by *ab initio* calculations^{28,69–74} and by experiments.^{75–77}

Whereas $E_{\text{elst+ind}}$ is rather small for benzene dimer, it grows in magnitude for larger acene dimers.³⁰ Even for $(\text{C}_6\text{H}_6)_2$, electrostatics makes an important contribution in that it provides an attractive driving force to decrease the intermolecular separation, once offset stacking has reduced the Pauli repulsion. The cofacial distance in $(\text{C}_6\text{H}_6)_2$ decreases from 3.8 Å in the sandwich isomer to 3.4 Å in the parallel-displaced isomer, the latter value being consistent with the 3.35 Å interlayer spacing in graphene.⁹² This effect generalizes to larger polycyclic aromatic hydrocarbons (PAHs) with larger stacking energies, and the general picture that emerges is that π -stacking is attributable to the fact that both electrostatics and dispersion are enhanced in cofacial geometries. This mechanism requires a close approach of the carbon rings and is therefore available to planar aromatic moieties but not to saturated hydrocarbons such as the cyclohexane-based perhydroacenes, which can also form stacked complexes.⁹³ This observation has been called the “pizza- π ” model of stacking,³⁰ although the π - π interaction really has more to do with the pizza (molecular shape) than with the π (aromaticity). This explains previous observations of strong stacking interactions between molecules that are planar but not aromatic.⁹⁴ Nowhere in this rationale is it necessary (or appropriate) to invoke a multipolar picture of electrostatics.

3.3. Myth: The Buckybowl Dipole Moment Drives Flexo-Electric Packing. A rather different example of π -stacking is the corannulene dimer, $(\text{C}_{20}\text{H}_{10})_2$, whose equilibrium structure is shown in Figure 6a. Unlike PAHs composed strictly

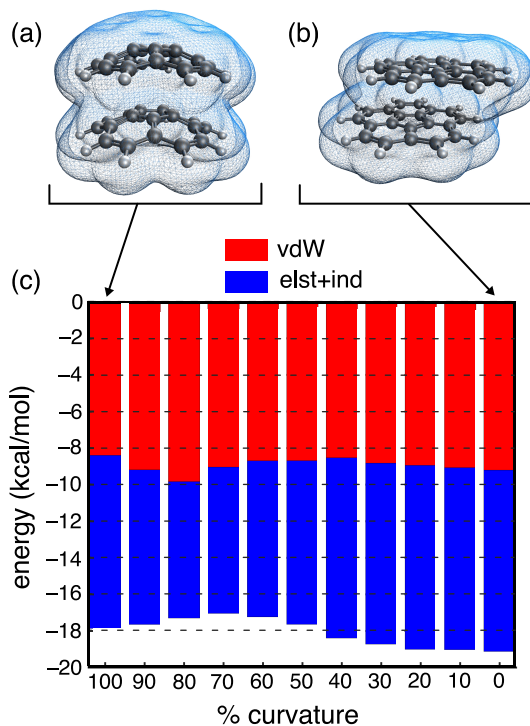


Figure 6. Corannulene dimer in (a) its equilibrium buckybowl geometry, where each monomer exhibits a dipole moment $\mu = 2.1$ D, vs (b) the structure obtained from a geometry optimization in which the monomers are constrained to be planar, with $\mu = 0$. Isocontours of the electron density ($\rho = 0.001$ au) are shown in each case. (c) Interaction energy along a curvature coordinate that connects the two structures, computed using XSAPT+MBD. The total length of each vertical bar (red + blue) indicates E_{int} for the geometry in question, which is decomposed according to $E_{\text{int}} = E_{\text{vdW}} + E_{\text{elst+ind}}$. Panel (c) is adapted from ref 30 with permission from the PCCP Owner Societies.

of hexagonal rings, the incorporation of one or more pentagons creates curvature,^{95–97} leading ultimately to the formation of fullerene buckyballs or buckytubes when the structure is closed. Corannulene and related materials with exposed concave

surfaces exhibit crystal packing consisting of concentric “buckybowls”,^{97–99} with the dimer in Figure 6a as the simplest example. These materials are of interest for organic electronics applications,⁹⁹ and a general feature is a pronounced “flexo-electric” effect,¹⁰⁰ wherein the molecule exhibits a dipole moment whose magnitude increases with the degree of curvature. Nanoscale PAHs can exhibit dipole moments in excess of 10 D as a result of this curvature.^{100,101}

The dipole moment of corannulene monomer in the gas phase has been measured at 2.07 D,¹⁰² and it has been suggested that dipole–dipole interactions compensate for the (presumed) loss of dispersion interactions in the curved framework of (C₂₀H₁₀)₂.¹⁰³ Corannulene is observed to form a stronger adduct with proteins as compared to the planar perylene molecule, which has been attributed to corannulene’s dipole moment.¹⁰⁴ In view of the misattribution of π – π conformational preferences to quadrupolar interactions, it seems pertinent to examine this attribution in more detail.

Figure 6c investigates the interaction energy of a corannulene dimer along a flexing coordinate that connects the concentric buckybowl equilibrium geometry (Figure 6a) to a structure in which the monomers are each constrained to be planar (Figure 6b). Isocontours of the charge density are shown for both end-point structures, using an isovalue that is often taken as a realistic description of molecular size.¹⁰⁵ These plots make it clear that the equilibrium stacking distance is well within the region of charge penetration where the two monomer densities exhibit significant overlap.

In the minimum-energy buckybowl geometry, the curved corannulene monomers each exhibit dipole moments $\mu = 2.1$ D,¹⁰⁶ oriented in the direction of the hydrogen-terminated side of the molecule. The dipole moment vanishes for the planar monomers, which adopt an offset-stacked geometry.^{30,103} Despite the disappearance of the dipole moment along the flexing coordinate, the value of E_{int} changes by only 1.2 kcal/mol between the two end-point structures in Figure 6, and in fact E_{int} is more stabilizing when the monomers are planar! (This is not enough to compensate for the monomer deformation penalty, however, so the binding energy of the complex is larger in the curved buckybowl geometry.) The polarized electrostatics energy also changes by only about 1 kcal/mol along the flexing coordinate in Figure 6, and it is more attractive (by ≈ 0.5 kcal/mol) when the monomers are planar. The dipole moment induced by flexing therefore does not enhance electrostatic interactions, as has previously been claimed.¹⁰⁷

The total interaction energy in Figure 6c is partitioned as $E_{\text{int}} = E_{\text{elst+ind}} + E_{\text{vdW}}$, and in fact both components are fairly well-balanced across the whole flexing coordinate, so the flexing-induced dipole moment also does not explain the stacking interaction. This interaction can be explained within the pizza- π model, however.³⁰ Despite the curvature, the interaction is still driven by molecular shape, because even curved arene monomers experience an enhanced electrostatic attraction as they approach at closer separation than is possible for aliphatic hydrocarbons. In the case of corannulene, this close approach is possible in either a planar cofacial arrangement or as nested buckybowls, and $E_{\text{elst+ind}}$ is largely indifferent to this choice. The curvature in the minimum-energy geometry is a result of internal strain within the monomers and is unrelated to noncovalent forces.

For corannulene dimer, the leading-order multipolar picture is doubly wrong. First, the structure with planar monomers (rather than buckybowls) has the more attractive value of

$E_{\text{elst+ind}}$, despite the fact that $\mu = 0$ for a planar corannulene monomer. Second, a vanishing dipole moment leaves the quadrupole–quadrupole interaction as the leading-order multipolar term, and that interaction is repulsive, just as it is for the cofacial isomer of benzene dimer. Nevertheless, electrostatic interactions are attractive at the 3.7 Å separation that characterizes (corannulene)₂ with planar monomers.¹⁰⁶ Corannulene dimer represents an even more egregious violation of the Hunter-Sanders paradigm as compared to a benzene dimer, because the quadrupole moment of corannulene is more than twice as large as that of benzene.¹⁰⁶

The deceptive nature of the corannulene dipole moment extends to other systems as well, such as the (corannulene)⋯(H₂O) complex whose gas-phase structure was recently determined via microwave spectroscopy and *ab initio* calculations.¹⁰⁸ Two isomers of this complex are shown in Figure 7,

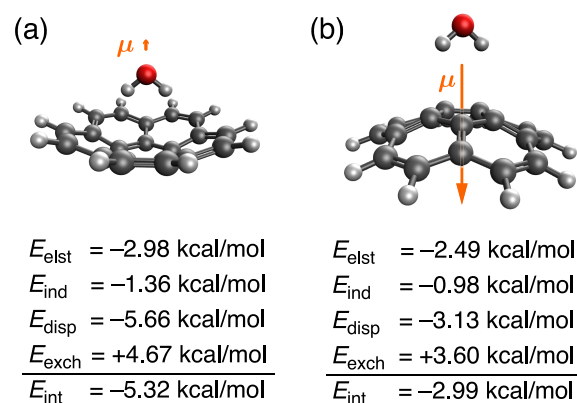


Figure 7. Isomers of (corannulene)⋯(H₂O): (a) “water inside” isomer with $\mu = 0.4$ D and (b) “water outside” isomer with $\mu = 5.1$ D, with geometries computed at the MP2/jun-cc-pVDZ level. Only the more stable isomer in (a) is observed in a supersonic expansion, whereas the binding energy of (b) is estimated to be 1.6 kcal/mol smaller.¹⁰⁸ Interaction energies were computed at the SAPT0+ δE_{HF} /jun-cc-pVDZ level.

although only the “inside” isomer (Figure 7a) is observed in the supersonic expansion. In that structure, the dipole moment vectors of the two monomers are oriented in an antiparallel fashion, leading to a net dipole moment of 0.4 D for the supramolecular complex. In the alternative “outside” isomer (Figure 7b), the monomer dipole moments add constructively, and the net dipole moment is $\mu = 5.1$ D for the complex, yet the binding energy is computed to be 1.6 kcal/mol smaller as compared to the inside isomer.¹⁰⁸ (Another common electrostatic fallacy in chemistry textbooks is to draw dipole moment vectors that point in the wrong direction.^{21,109} The vectors μ in Figure 7 are consistent with electropositive C–H bonds for corannulene.)

SAPT analysis (Figure 7) suggests that both E_{elst} and E_{ind} are more attractive for the structure whose monomer dipole moments are antiparallel. (The same conclusion is borne out by partial third-order SAPT calculations.¹⁰⁸) In the “inside” isomer, the water molecule is only slightly closer to the nearest carbon atom (by $\lesssim 0.1$ Å) as compared to the “outside” isomer, but the greater number of close-contact carbon atoms in the former enhances the Pauli repulsion. This is offset by a combination of polarized electrostatics and dispersion, both of which are more attractive for the inside isomer. The picture that

one might assume based on a dipole-centric view of electrostatics is completely opposite to experiment and theory.

3.4. Myth: Ion–Dipole Interactions Drive Halide–Water Binding. The final systems considered here are binary halide–water complexes, $X^-(\text{H}_2\text{O})$. In an aqueous solution, monodentate solvation of the halide ions (i.e., one O–H moiety per water molecule) has long been inferred based on neutron and X-ray diffraction studies as well as infrared spectroscopy,¹¹⁰ and this picture was recently reaffirmed via X-ray absorption spectroscopy.¹¹¹ Vibrational spectroscopy of $X^-(\text{H}_2\text{O})_n$ clusters is also consistent with monodentate rather than bidentate coordination,^{112–114} which is confirmed by *ab initio* calculations.^{115–121} Molecular dynamics simulations of $X^-(\text{aq})$, using polarizable force fields fitted to *ab initio* calculations, find that average $X^-\cdots\text{H}-\text{O}$ bond angles for first-shell water molecules are within 7° of linear for $X = \text{Cl}, \text{Br}, \text{and I}$.¹²² This picture is consistent with the formation of ion–water hydrogen bonds but inconsistent with the bidentate C_{2v} -symmetric solvation motif that is suggested by ion–dipole considerations. Both motifs are shown in Figure 8, which also defines the angle θ_{XOH} that is used in the energy profiles reported below.

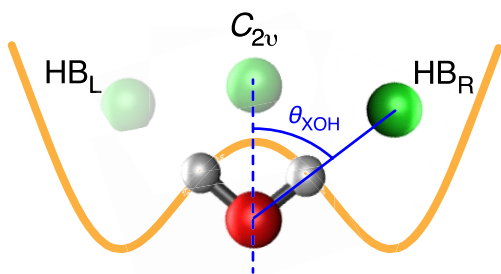


Figure 8. Diagram of the $X^-\cdots\text{H}-\text{O}$ angle (θ_{XOH}) for the halide–water complex $X^-(\text{H}_2\text{O})$. As indicated by the potential energy curve shown in the background, the C_{2v} structure is an energetic saddle point between left and right hydrogen-bonded isomers. Adapted from ref 36, copyright 2021 American Chemical Society.

The charge–dipole interaction in $X^-(\text{H}_2\text{O})$ is considerably larger than the leading-order quadrupolar interaction in the benzene dimer or the dipolar interaction in (corannulene) $\cdots(\text{H}_2\text{O})$, so it is worth exploring whether this might be a case where the multipolar picture remains valid even at close-contact distances. It is not such a case, as is immediately evident upon examining the electrostatic energy profile $E_{\text{elst}}(\theta_{\text{XOH}})$ in Figure 9, which indicates that electrostatics is most attractive in hydrogen-bonded geometries. The total interaction energy profile, $E_{\text{int}}(\theta_{\text{XOH}})$, forms a symmetric double well with a C_{2v} saddle point separating hydrogen-bonded minima. (A small cusp in E_{int} at $\theta_{\text{XOH}} = 0$ arises from an avoided crossing in coordinate space and disappears if the H_2O relaxation energy is included.³⁶) Even electrostatics, when computed using monomer charge densities rather than any multipolar approximation, disfavors the C_{2v} “dipole geometry”.

For Cl^- and larger halides, the double-well potential is nearly flat,³⁶ as shown for $\text{Cl}^-(\text{H}_2\text{O})$ in Figure 9b, although even in $\text{I}^-(\text{H}_2\text{O})$ it is possible to measure tunneling splittings,¹²³ meaning that a left \leftrightarrow right barrier must still exist. The simple charge–dipole picture suggests that $E_{\text{int}}(\theta_{\text{XOH}})$, or at least $E_{\text{elst}}(\theta_{\text{XOH}})$, should have a minimum at $\theta_{\text{XOH}} = 0$, but no such minimum is observed even for Br^- .³⁶ This implies that the leading-order multipolar approximation provides a poor description of E_{elst} let alone E_{int} , even for the larger halides.

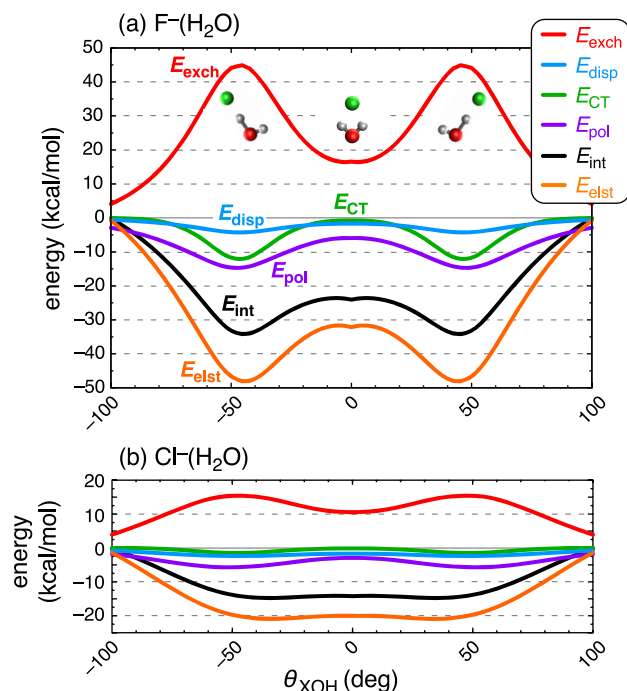


Figure 9. Total interaction energy (E_{int}) and components thereof for (a) $\text{F}^-(\text{H}_2\text{O})$ and (b) $\text{Cl}^-(\text{H}_2\text{O})$, along radial scans of the $X^-\cdots\text{H}-\text{O}$ angle defined in Figure 8. All other geometric degrees of freedom are relaxed at each value of θ_{XOH} , and the cartoon structures in (a) emphasize the asymmetry of the O–H bond lengths in the hydrogen-bonded geometries. Calculations were performed at the level of SAPT0+ δE_{HF} /jun-cc-pVDZ(-PP). Adapted from ref 36, copyright 2021 American Chemical Society.

As evident from Figure 9, the Pauli repulsion is maximally repulsive at the hydrogen-bonded geometries, for which the ion is closer to the water molecule than it is in the C_{2v} geometry. A minimalist model for this system might therefore consist of electrostatics plus finite size ($E_{\text{elst}} + E_{\text{exch}}$), and this potential is plotted for $\text{F}^-(\text{H}_2\text{O})$ and $\text{Cl}^-(\text{H}_2\text{O})$ in Figure 10. The global minimum in $E_{\text{elst}} + E_{\text{exch}}$ is found at the C_{2v} geometry, consistent with the classical ion–dipole picture, although in the case of $\text{F}^-(\text{H}_2\text{O})$ there remain shallow local minima corresponding to hydrogen bonding. These are absent for Cl^- and larger halide ions.

Unlike other systems considered here, the induction energy is sizable for $X^-(\text{H}_2\text{O})$ and warrants a careful discussion. This is a case where it is conceptually useful to separate induction into polarization and CT components (eq 8), because charge donation into water’s σ^* orbitals has long been considered to provide a mechanism for O–H vibrational redshifts associated with hydrogen bonding.^{124–131} Indeed, “fractional covalency” has been suggested as an essential aspect of the hydrogen bond,¹³² although estimates of the fraction vary considerably depending on the particular EDA that is used.¹³³ Extreme vibrational redshifts are observed in small anion–water complexes,^{112–114} and the $X^- \rightarrow \sigma_{\text{OH}}^*$ charge-donation mechanism is supported by theoretical calculations.^{134–136}

The CT component of the induction energy can be isolated using a procedure based on charge-constrained DFT (cDFT).^{34–36} Originally developed for other purposes,¹³⁷ cDFT can be used in the present context to define a CT-free reference state in which monomers A and B are allowed to polarize one another, but the integrated charge density

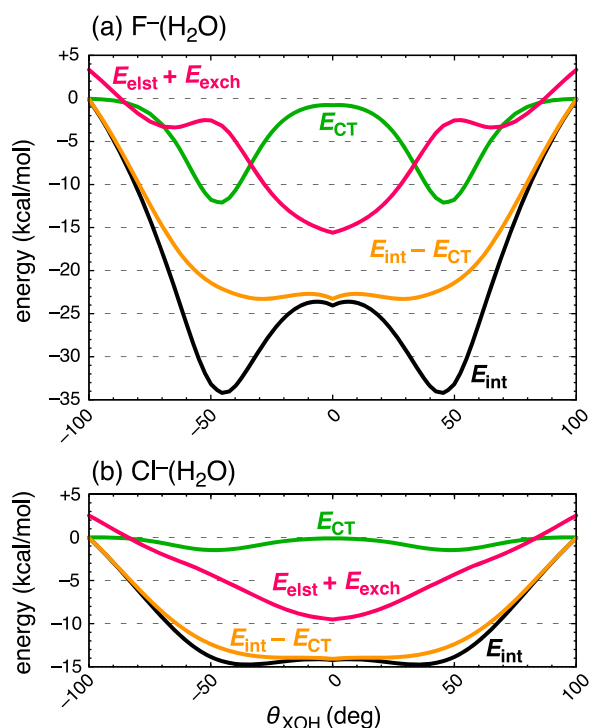


Figure 10. Total interaction energies and some components thereof for (a) $\text{F}^-(\text{H}_2\text{O})$ and (b) $\text{Cl}^-(\text{H}_2\text{O})$, demonstrating the effect of removing the CT component of the interaction energy. Computational details are the same as in Figure 9. Data were taken from ref 36.

$$N_A = \int w_A(\mathbf{r}) \rho^A(\mathbf{r}) \, d\mathbf{r} \quad (13)$$

is constrained to be an integer, with $w_A(\mathbf{r})$ as a suitable weight function.³⁶ The procedure is variational, and the energy lowering upon lifting of the charge constraint, which allows N_A to take fractional values, defines the CT energy, E_{CT} . The “true” (or CT-free) polarization energy E_{pol} is taken to be the remainder of the SAPT induction energy, as suggested by eq 8. Importantly, this cDFT-based definition of E_{CT} is stable with respect to changes in the underlying Gaussian basis set, whereas many alternative definitions are not.³⁵

In the case of $\text{X}^-(\text{H}_2\text{O})$, separation of E_{CT} provides a compelling narrative for the formation of quasi-linear hydrogen bonds, as demonstrated for $\text{F}^-(\text{H}_2\text{O})$ and $\text{Cl}^-(\text{H}_2\text{O})$ in Figure 10. The energy profile defined by $E_{\text{int}} - E_{\text{CT}}$ (as a function of the angle θ_{XOH}) is essentially flat, showing no preference for hydrogen bonding. Importantly, this is still inconsistent with the charge–dipole description, which would predict a proper minimum at the C_{2v} geometry, because nonzero values of θ_{XOH} orient the dipole moment vector away from the ion. The CT energy turns on sharply near quasi-linear $\text{X}^-\cdots\text{H}-\text{O}$ geometries, which can be understood in terms of orbital overlap between the X^- lone pair (donor orbital) and the σ_{OH}^* acceptor orbital. It is this CT energy component that is responsible for the double well. A more nuanced analysis, which compares results for relaxed versus unrelaxed H_2O geometries, can be found in ref 36.

Note that E_{CT} exerts an important influence on the conformational preferences of $\text{X}^-(\text{H}_2\text{O})$ despite the fact that its magnitude is small compared to either E_{elst} or E_{exch} . This observation (along with the analysis of $\pi-\pi$ conformational preferences in Section 3.2) highlights the importance of examining the potential energy landscape, rather than simply

applying an EDA at minimum-energy geometries. The diminutive magnitude of the CT term in $(\text{H}_2\text{O})_2$ has led to a suggestion that hydrogen bonding is dominated by electrostatics,¹³⁸ which may be literally true in a numerical sense, but “dominated by” is not the same as “driven by”. Conclusions regarding how particular energy components influence molecular and supramolecular structures cannot properly be drawn without examination of a potential energy surface.

4. WHERE DO WE GO FROM HERE?

Examples discussed herein document the abject failure of the single-center multipole expansion to explain intermolecular phenomena at typical nonbonded close-contact distances. From a certain (mathematical) point of view, this is not so very surprising, as the multipole moments are defined by an asymptotic expansion that is known to diverge at short range. It is only surprising from the point of view of someone reared in a curriculum that routinely engages in gross oversimplification, to the point that it seems (to this author, at least) that greater value is often placed on simplicity than on correctness. A guiding principle for textbooks could be “omission before oversimplification”,¹³⁹ but this does not seem to be the norm in modern chemical education.

At least for the noncovalent phenomena discussed herein, a way forward has been clear for a long time: abandon the single-center multipole expansion in favor of a “distributed” multipole analysis,²⁷ as championed by Stone.^{21,140} Using multipoles that are atom- or bond-centered, one can obtain a quantitative description of electrostatics using only low-order moments, preserving qualitative interpretability. This approach is already widely used to parametrize polarizable force fields,^{141–145} and SAPT calculations have also been used to parametrize force fields whose energy components are physically meaningful.^{146–150} The distributed-multipole approach is consistent with the qualitative idea of a bond dipole yet computable from electronic structure calculations in a rigorous and well-defined way. While such approaches are at the forefront of modern force-field development,^{150–152} they have received little (if any) attention in chemical education. Perhaps it is time for that to change.

■ AUTHOR INFORMATION

Corresponding Author

John M. Herbert – Department of Chemistry and Biochemistry, The Ohio State University, Columbus, Ohio 43210, United States; orcid.org/0000-0002-1663-2278; Email: herbert@chemistry.ohio-state.edu

Complete contact information is available at: <https://pubs.acs.org/10.1021/acs.jpca.1c05962>

Notes

The author declares no competing financial interest.

Biography



John M. Herbert is a quantum chemist with wide-ranging interests in physical chemistry. In addition to noncovalent interactions, these include solvation modeling, condensed-phase spectroscopy, photochemistry, and the electron correlation problem. His work focuses on the development of new methods and algorithms, and his research group is a major contributor to the Q-Chem electronic structure program. He is a past recipient of fellowships from the Humboldt, Dreyfus, and Sloan Foundations, and currently holds the rank of Professor at The Ohio State University.

ACKNOWLEDGMENTS

This work was supported by the United States Department of Energy, Office of Basic Energy Sciences, Division of Chemical Sciences, Geosciences, and Biosciences under Award No. DE-SC0008550.

REFERENCES

- Bertozzi, C. R. The centrality of chemistry. *ACS Cent. Sci.* **2015**, *1*, 1–2.
- Roth, D. L. Several centuries of centrality. *ACS Cent. Sci.* **2015**, *1*, 103–105.
- Balaban, A. T.; Klein, D. J. Is chemistry “The Central Science”? How are different sciences related? Co-citations, reductionism, emergence, and posets. *Scientometrics* **2006**, *69*, 615–637.
- Ellis, G. F. R. Physics and the real world. *Phys. Today* **2005**, *58*, 49–54.
- Blackett, P. M. S. Memories of Rutherford. In *Rutherford at Manchester*; Birks, J. B., Ed.; Heywood & Co.: London, UK, 1962.
- Anderson, P. W. More is different. *Science* **1972**, *177*, 393–396.
- Anderson, P. W. More is different—one more time. In *More Is Different: Fifty Years of Condensed Matter Physics*; Ong, N. P., Bhatt, R. N., Eds.; Princeton Series in Physics Princeton University Press: Princeton, NJ, 2001.
- Peterson, K. A.; Dunning, T. H., Jr. The CO molecule: The role of basis set and correlation treatment in the calculation of molecular properties. *J. Mol. Struct.: THEOCHEM* **1997**, *400*, 93–117.
- Herbert, J. M. The quantum chemistry of loosely-bound electrons. In *Reviews in Computational Chemistry*; Parill, A. L., Lipkowitz, K., Eds.; Wiley-VCH: Hoboken, NJ, 2015; Vol. 28 pp 391–517.
- Hotop, H.; Lineberger, W. C. Binding energies in atomic negative ions: II. *J. Phys. Chem. Ref. Data* **1985**, *14*, 731–750.
- Electron affinities for F and Cl predicted at the CCSD(T)/aug-cc-pVQZ level are 3.38 and 3.61 eV, respectively, in comparison to experimental values of 3.40 and 3.62 eV.¹⁰ These quantities are amenable to good theory (as is the dipole moment of CO),⁸ whether or not a simple explanation exists.
- Hohenstein, E. G.; Sherrill, C. D. Wavefunction methods for noncovalent interactions. *WIREs Comput. Mol. Sci.* **2012**, *2*, 304–326.
- Szalewicz, K. Symmetry-adapted perturbation theory of intermolecular forces. *WIREs Comput. Mol. Sci.* **2012**, *2*, 254–272.
- Jansen, G. Symmetry-adapted perturbation theory based on density functional theory for noncovalent interactions. *Wiley Interdiscip. Rev.: Comput. Mol. Sci.* **2014**, *4*, 127–144.
- Francisco, E.; Pendás, A. M. Energy partition analyses: Symmetry-adapted perturbation theory and other techniques. In *Non-Covalent Interactions in Quantum Chemistry and Physics*; de la Roza, A. O., DiLabio, G. A., Eds.; Elsevier: Amsterdam, Netherlands, 2017; pp 27–64.
- Carter-Fenk, K.; Lao, K. U.; Herbert, J. M. Predicting and understanding noncovalent interactions using novel forms of symmetry-adapted perturbation theory. *Acc. Chem. Res.* (submitted).2021
- Patkowski, K. Recent developments in symmetry-adapted perturbation theory. *Wiley Interdiscip. Rev.: Comput. Mol. Sci.* **2020**, *10*, e1452.
- Jeziorski, B.; Moszynski, R.; Szalewicz, K. Perturbation theory approach to intermolecular potential energy surfaces of van der Waals complexes. *Chem. Rev.* **1994**, *94*, 1887–1930.
- Kaplan, I. G.; Rodimova, O. B. Intermolecular interactions. *Sov. Phys. Usp.* **1978**, *21*, 918–943.
- Kaplan, I. G. *Intermolecular Interactions: Physical Picture, Computational Methods and Model Potentials*; John Wiley & Sons: Chichester, United Kingdom, 2006.
- Stone, A. J. *The Theory of Intermolecular Forces*, 2nd ed.; Oxford University Press: Oxford, UK, 2013.
- Stone, A. J. Physical basis of intermolecular interactions. In *Non-Covalent Interactions in Quantum Chemistry and Physics*; de la Roza, A. O., DiLabio, G. A., Eds.; Elsevier: Amsterdam, Netherlands, 2017; pp 3–26.
- The terms identified as E_{elst} and E_{exch} in eq 1 appear at first order in SAPT, including all three components of E_{elst} in eq 2. To make contact with the detailed treatment in ref 18, one should identify $E_{\text{elst}} \equiv E_{\text{pol}}^{(1)}$ and $E_{\text{exch}} \equiv E_{\text{exch}}^{(1)}$.
- Induction and dispersion appear at second order in SAPT and are accompanied by exchange-induction and exchange-dispersion terms,¹⁸ which reduce their magnitude relative to the corresponding terms in the long-range polarization expansion. In the present work, the induction and exchange-induction are grouped together and called E_{ind} , with a similar convention for E_{disp} .
- Gray, C. G.; Gubbins, K. E. *Theory of Molecular Fluids, Fundamentals*; Oxford University Press: New York, 1984; Vol. I.
- Stone, A. J. Classical electrostatics in molecular interactions. In *Theoretical Treatment of Large Molecules and Their Interactions*; Maksić, Z. B., Ed.; Springer-Verlag: Berlin, Germany, 1991; pp 103–131.
- Vigné-Maeder, F.; Claverie, P. The exact multicenter multipolar part of a molecular charge distribution and its simplified representations. *J. Chem. Phys.* **1988**, *88*, 4934–4948.
- Sherrill, C. D. Energy component analysis of π interactions. *Acc. Chem. Res.* **2013**, *46*, 1020–1028.
- Ryno, S. M.; Risko, C.; Brédas, J.-L. Noncovalent interactions and impact of charge penetration effects in linear oligoacene dimers and single crystals. *Chem. Mater.* **2016**, *28*, 3990–4000.
- Carter-Fenk, K.; Herbert, J. M. Reinterpreting π -stacking. *Phys. Chem. Chem. Phys.* **2020**, *22*, 24870–24886.
- Antisymmetrization of the reference state or “strong symmetry forcing” is reviewed in ref 18, but it is computationally challenging and has never been deployed in a widespread way. The “weak symmetry forcing” variant is nowadays synonymous with SAPT.
- Smith, D. W. A simple molecular orbital treatment of the barrier to internal rotation in the ethane molecule. *J. Chem. Educ.* **1998**, *75*, 907–909.
- Misquitta, A. J. Charge transfer from regularized symmetry-adapted perturbation theory. *J. Chem. Theory Comput.* **2013**, *9*, 5313–5326.
- Rezáč, J.; de la Lande, A. Robust, basis-set independent method for the evaluation of charge-transfer energy in noncovalent complexes. *J. Chem. Theory Comput.* **2015**, *11*, 528–537.

- (35) Lao, K. U.; Herbert, J. M. Energy decomposition analysis with a stable charge-transfer term for interpreting intermolecular interactions. *J. Chem. Theory Comput.* **2016**, *12*, 2569–2582.
- (36) Herbert, J. M.; Carter-Fenk, K. Electrostatics, charge transfer, and the nature of the halide–water hydrogen bond. *J. Phys. Chem. A* **2021**, *125*, 1243–1256.
- (37) London, F. The general theory of intermolecular forces. *Trans. Faraday Soc.* **1937**, *33*, 8–26.
- (38) Truhlar, D. G. Dispersion forces: Neither fluctuating nor dispersing. *J. Chem. Educ.* **2019**, *96*, 1671–1675.
- (39) Chemistry textbooks generally favor “London forces” over “dispersion forces”, perhaps to avoid the technicalities of the metaphor that is described in ref 38. London’s derivation involved simplifying assumptions, and more complete versions were given later by others; see ref 40 for a discussion.
- (40) Longuet-Higgins, H. C. Intermolecular forces. *Discuss. Faraday Soc.* **1965**, *40*, 7–18.
- (41) Clerk-Maxwell, J. Van der Waals on the continuity of the gaseous and liquid states. *Nature* **1874**, *10*, 477–480.
- (42) Carter-Fenk, K.; Herbert, J. M. Electrostatics does not dictate the slip-stacked arrangement of aromatic π – π interactions. *Chem. Sci.* **2020**, *11*, 6758–6765.
- (43) Wagner, J. P.; Schreiner, P. R. London dispersion in molecular chemistry—Reconsidering steric effects. *Angew. Chem., Int. Ed.* **2015**, *54*, 12274–1229.
- (44) Phipps, M. J. S.; Fox, T.; Tautermann, C. S.; Skylaris, C.-K. Energy decomposition analysis approaches and their evaluation on prototypical protein–drug interaction patterns. *Chem. Soc. Rev.* **2015**, *44*, 3177–3211.
- (45) Zhao, L.; von Hopffgarten, M.; Andrada, D. M.; Frenking, G. Energy decomposition analysis. *Wiley Interdiscip. Rev.: Comput. Mol. Sci.* **2018**, *8*, No. e1345.
- (46) Andrés, J.; Ayers, P. W.; Boto, R. A.; Carbó-Dorca, R.; Chermette, H.; Cioslowski, J.; Contreras-García, J.; Cooper, D. L.; Frenking, G.; Gatti, C.; et al. Nine questions on energy decomposition analysis. *J. Comput. Chem.* **2019**, *40*, 2248–2283.
- (47) Grimme, S. Density functional theory with London dispersion corrections. *Wiley Interdiscip. Rev.: Comput. Mol. Sci.* **2011**, *1*, 211–228.
- (48) Grimme, S.; Hansen, A.; Brandenburg, J. G.; Bannwarth, C. Dispersion-corrected mean-field electronic structure methods. *Chem. Rev.* **2016**, *116*, 5105–5154.
- (49) Grimme, S. Semiempirical GGA-type density functional constructed with a long-range dispersion correction. *J. Comput. Chem.* **2006**, *27*, 1787–1799.
- (50) Shahbaz, M.; Szalewicz, K. Do semilocal density-functional approximations recover dispersion energies at small intermonomer separations? *Phys. Rev. Lett.* **2018**, *121*, 113402.
- (51) Price, A. J. A.; Bryenton, K. R.; Johnson, E. R. Requirements for an accurate dispersion-corrected density functional. *J. Chem. Phys.* **2021**, *154*, 230902.
- (52) van Duijneveldt, F. B.; van Duijneveldt-van de Rijdt, J. G. C. M.; van Lenthe, J. H. State of the art in counterpoise theory. *Chem. Rev.* **1994**, *94*, 1873–1885.
- (53) Parker, T. M.; Burns, L. A.; Parrish, R. M.; Ryno, A. G.; Sherrill, C. D. Levels of symmetry adapted perturbation theory (SAPT). I. Efficiency and performance for interaction energies. *J. Chem. Phys.* **2014**, *140*, 094106.
- (54) Szalewicz, K.; Patkowski, K.; Jeziorski, B. Intermolecular interactions via perturbation theory: From diatoms to biomolecules. In *Intermolecular Forces and Clusters II*; Wales, D. J., Ed.; Springer-Verlag: Berlin, Germany, 2005; Vol. 116, pp 43–117.
- (55) Lao, K. U.; Herbert, J. M. Accurate intermolecular interactions at dramatically reduced cost: XPol+SAPT with empirical dispersion. *J. Phys. Chem. Lett.* **2012**, *3*, 3241–3248.
- (56) Lao, K. U.; Herbert, J. M. An improved treatment of empirical dispersion and a many-body energy decomposition scheme for the explicit polarization plus symmetry-adapted perturbation theory (XSAPT) method. *J. Chem. Phys.* **2013**, *139*, 034107. Erratum: *J. Chem. Phys.* **2014**, *140*, 119901.
- (57) Lao, K. U.; Herbert, J. M. Accurate and efficient quantum chemistry calculations of noncovalent interactions in many-body systems: The XSAPT family of methods. *J. Phys. Chem. A* **2015**, *119*, 235–253.
- (58) Lao, K. U.; Herbert, J. M. Atomic orbital implementation of extended symmetry-adapted perturbation theory (XSAPT) and benchmark calculations for large supramolecular complexes. *J. Chem. Theory Comput.* **2018**, *14*, 2955–2978.
- (59) Liu, K.-Y.; Carter-Fenk, K.; Herbert, J. M. Self-consistent charge embedding at very low cost, with application to symmetry-adapted perturbation theory. *J. Chem. Phys.* **2019**, *151*, 031102.
- (60) Carter-Fenk, K.; Lao, K. U.; Liu, K.-Y.; Herbert, J. M. Accurate and efficient *ab initio* calculations for supramolecular complexes: Symmetry-adapted perturbation theory with many-body dispersion. *J. Phys. Chem. Lett.* **2019**, *10*, 2706–2714.
- (61) Gray, M.; Herbert, J. M. Simplified tuning of long-range corrected density functionals for symmetry-adapted perturbation theory. *J. Chem. Phys.* **2021**, *155*, 034103.
- (62) Herbert, J. M.; Jacobson, L. D.; Un Lao, K.; Rohrdanz, M. A. Rapid computation of intermolecular interactions in molecular and ionic clusters: Self-consistent polarization plus symmetry-adapted perturbation theory. *Phys. Chem. Chem. Phys.* **2012**, *14*, 7679–7699.
- (63) Bickelhaupt, F. M.; Baerends, E. J. Kohn-Sham density functional theory: Predicting and understanding chemistry. In *Reviews in Computational Chemistry*; Lipkowitz, K. B.; Boyd, D. B., Eds.; Wiley-VCH: New York, 2000; Vol. 15.
- (64) Hunter, C. A.; Sanders, J. K. M. The nature of π – π interactions. *J. Am. Chem. Soc.* **1990**, *112*, 5525–5534.
- (65) Fleming, I. *Molecular Orbitals and Organic Chemical Reactions*; John Wiley & Sons: Chichester, United Kingdom, 2010.
- (66) Fagnani, D. E.; Sotuyo, A.; Castellano, R. K. π – π interactions. In *Comprehensive Supramolecular Chemistry II*; Elsevier: Oxford, UK, 2017; Vol. 1, pp 121–148.
- (67) Sinnokrot, M. O.; Sherrill, C. D. Substituent effects in π – π interactions: Sandwich and T-shaped configurations. *J. Am. Chem. Soc.* **2004**, *126*, 7690–7697.
- (68) Podeszwa, R.; Bukowski, R.; Szalewicz, K. Potential energy surface for the benzene dimer and perturbational analysis of π – π interactions. *J. Phys. Chem. A* **2006**, *110*, 10345–10354.
- (69) Wheeler, S. E.; Houk, K. N. Substituent effects in the benzene dimer are due to direct interactions of the substituents with the unsubstituted benzene. *J. Am. Chem. Soc.* **2008**, *130*, 10854–10855.
- (70) Wheeler, S. E.; Houk, K. N. Through-space effects of substituents dominate molecular electrostatic potentials of substituted arenes. *J. Chem. Theory Comput.* **2009**, *5*, 2301–2312.
- (71) Wheeler, S. E.; Houk, K. N. Origin of substituent effects in edge-to-face aryl–aryl interactions. *Mol. Phys.* **2009**, *107*, 749–760.
- (72) Wheeler, S. E. Local nature of substituent effects in stacking interactions. *J. Am. Chem. Soc.* **2011**, *133*, 10262–10274.
- (73) Raju, R. K.; Bloom, J. W. G.; Wheeler, S. E. Broad transferability of substituent effects in π -stacking interactions provides new insights into their origin. *J. Chem. Theory Comput.* **2013**, *9*, 3479–3490.
- (74) Parrish, R. M.; Sherrill, C. D. Quantum-mechanical evaluation of the π – π versus substituent– π interactions in π stacking: Direct evidence for the Wheeler–Houk picture. *J. Am. Chem. Soc.* **2014**, *136*, 17386–17389.
- (75) Snyder, S. E.; Huang, B.-S.; Chen, Y.-T.; Lin, H.-S.; Carey, J. R. A simple chiral recognition system to investigate substituent effects on π – π interactions. *Org. Lett.* **2012**, *14*, 3442–3445.
- (76) Snyder, S. E.; Huang, B.-S.; Chu, Y. W.; Lin, H.-S.; Carey, J. R. The effects of substituents on the geometry of π – π interactions. *Chem. - Eur. J.* **2012**, *18*, 12663–12671.
- (77) Hwang, J.; Li, P.; Carroll, W. R.; Smith, M. D.; Pellechia, P. J.; Shimizu, K. D. Additivity of substituent effects in aromatic stacking interactions. *J. Am. Chem. Soc.* **2014**, *136*, 14060–14067. Erratum: *J. Am. Chem. Soc.* **2019**, *141*, 4154.
- (78) Garcia, A. M.; Determan, J. J.; Janesko, B. G. Tunable fictitious substituent effects on the π – π interactions of substituted sandwich benzene dimers. *J. Phys. Chem. A* **2014**, *118*, 3344–3350.

- (79) Riwar, L.-J.; Trapp, N.; Kuhn, B.; Diederich, F. Substituent effects in parallel-displaced π - π stacking interactions: Distance matters. *Angew. Chem., Int. Ed.* **2017**, *56*, 11252–11257.
- (80) Cabaleiro-Lago, E. M.; Rodríguez-Otero, J. σ - σ , σ - π , and π - π stacking interactions between six-membered cyclic systems. Dispersion dominates and electrostatics commands. *ChemistrySelect* **2017**, *2*, 5157–5166.
- (81) Malenov, D. P.; Aladić, A. J.; Zarić, S. D. Stacking interactions of borazine: Important stacking at large horizontal displacements and dihydrogen bonding governed by electrostatic potentials of borazine. *Phys. Chem. Chem. Phys.* **2019**, *21*, 24554–24564.
- (82) Glova, A. D.; Larin, S. V.; Nazarychev, V. M.; Kenny, J. M.; Lyulin, A. V.; Lyulin, S. V. Toward predictive molecular dynamics simulations of asphaltenes in toluene and heptane. *ACS Omega* **2019**, *4*, 20005–20014.
- (83) Mousavi, M.; Fini, E. H. Non-covalent π -stacking interactions between asphaltene and porphyrin in bitumen. *J. Chem. Inf. Model.* **2020**, *60*, 4856–4866.
- (84) Battaglia, M. R.; Buckingham, A. D.; Williams, J. H. The electric quadrupole moments of benzene and hexafluorobenzene. *Chem. Phys. Lett.* **1981**, *78*, 421–423.
- (85) Sinnokrot, M. O.; Valeev, E. F.; Sherrill, C. D. Estimates of the ab initio limit for π - π interactions: The benzene dimer. *J. Am. Chem. Soc.* **2002**, *124*, 10887–10893.
- (86) Hunter, C. A.; Singh, J.; Thornton, J. M. π - π interactions: The geometry and energetics of phenylalanine-phenylalanine interactions in proteins. *J. Mol. Biol.* **1991**, *218*, 837–846.
- (87) Antony, J.; Grimme, S. Structures and interaction energies of stacked graphene–nucleobase complexes. *Phys. Chem. Chem. Phys.* **2008**, *10*, 2722–2729.
- (88) Gung, B. W.; Amicangelo, J. C. Substituent effects in C_6F_6 – C_6H_5X stacking interactions. *J. Org. Chem.* **2006**, *71*, 9261–9270.
- (89) Tsuzuki, S.; Uchimaru, T.; Mikami, M. Intermolecular interaction between hexafluorobenzene and benzene: Ab initio calculations including CCSD(T) level electron correlation correction. *J. Phys. Chem. A* **2006**, *110*, 2027–2033.
- (90) Wang, W.; Zhang, Y.; Wang, Y.-B. Highly accurate benchmark calculations of the interaction energies in the complexes $C_6H_6 \cdots C_6X_6$ ($X = F, Cl, Br, \text{ and } I$). *Int. J. Quantum Chem.* **2017**, *117*, No. e25345.
- (91) For a symmetric top, the traceless quadrupole moment tensor Θ has only one independent component ($\Theta_{zz} = -2\Theta_{xx} = -2\Theta_{yy}$),^{21,25} so one can speak of “the” quadrupole moment. The units for quadrupole moments are Buckingham (B), with $1 \text{ B} = 1 \text{ D} \text{ \AA}$.
- (92) Franklin, R. E. The structure of graphitic carbon. *Acta Crystallogr.* **1951**, *4*, 253–261.
- (93) For a given number of rings n , the T-shaped acene dimers ($C_{4n+2}H_{2n+4}$)₂ exhibit interaction energies that are systematically comparable to those of their cyclohexane-based analogues, the perhydroacene dimers ($C_{4n+2}H_{6n+6}$)₂.³⁰ That fact alone should dispel any lingering thoughts that acene–acene interactions are quadrupole-driven.
- (94) Bloom, J. W. G.; Wheeler, S. E. Taking the aromaticity out of aromatic interactions. *Angew. Chem., Int. Ed.* **2011**, *50*, 7847–7849.
- (95) Baldridge, K. K.; Siegel, J. S. Corannulene-based fullerene fragments $C_{20}H_{10}$ – $C_{50}H_{10}$: When does a bucky bowl become a buckytube? *Theor. Chem. Acc.* **1997**, *97*, 67–71.
- (96) Scott, L. T.; Bronstein, H. E.; Preda, D. V.; Ansems, R. B. M.; Bratcher, M. S.; Hagen, S. Geodesic polyarenes with exposed concave surfaces. *Pure Appl. Chem.* **1999**, *71*, 209–219.
- (97) Stuparu, M. C. Corannulene: A curved polyarene building block for the construction of functional materials. *Acc. Chem. Res.* **2021**, *54*, 2858–2870.
- (98) Hanson, J. C.; Nordman, C. E. The crystal and molecular structure of corannulene, $C_{20}H_{10}$. *Acta Crystallogr., Sect. B: Struct. Crystallogr. Cryst. Chem.* **1976**, *32*, 1147–1153.
- (99) Chen, R.; Lu, R.-Q.; Shi, P.-C.; Cao, X.-Y. Corannulene derivatives for organic electronics: From molecular engineering to applications. *Chin. Chem. Lett.* **2016**, *27*, 1175–1183.
- (100) Kvashnin, A. G.; Sorokin, P. B.; Yakobson, B. I. Flexoelectricity in carbon nanostructures: Nanotubes, fullerenes, and nanocones. *J. Phys. Chem. Lett.* **2015**, *6*, 2740–2744.
- (101) Martin, J. W.; Slavchov, R. I.; Yapp, E. K. Y.; Akroyd, J.; Mosbach, S.; Kraft, M. The polarization of polycyclic aromatic hydrocarbons curved by pentagon incorporation: The role of the flexoelectric dipole. *J. Phys. Chem. C* **2017**, *121*, 27154–27163.
- (102) Lovas, F. J.; McMahon, R. J.; Grabow, J.-U.; Schnell, M.; Mack, J.; Scott, L. T.; Kuczkowski, R. L. Interstellar chemistry: A strategy for detecting polycyclic aromatic hydrocarbons in space. *J. Am. Chem. Soc.* **2005**, *127*, 4345–4349.
- (103) Sygula, A.; Saebø, S. π - π stacking of curved carbon networks: The corannulene dimer. *Int. J. Quantum Chem.* **2009**, *109*, 65–72.
- (104) Du, S.; Wang, H.; Yang, Y.; Feng, X.; Shao, X.; Chipot, C.; Cai, W. Curvature of bucky bowl corannulene enhances its binding to proteins. *J. Phys. Chem. C* **2019**, *123*, 922–930.
- (105) Herbert, J. M. Dielectric continuum methods for quantum chemistry. *Wiley Interdiscip. Rev.: Comput. Mol. Sci.* **2021**, *11*, e1519.
- (106) In its curved equilibrium geometry, the corannulene monomer exhibits a dipole moment of 2.1 D and a quadrupole moment⁹¹ of 17.0 B at the TPSS+D3/def2-TZVP level of theory that was used for geometry optimizations. (The planar monomer has a quadrupole moment of 20.8 B.) At that level of theory, the equilibrium intermolecular separation of (corannulene)₂ is 3.7 Å. For comparison, the same level of theory affords an eclipsed-cofacial isomer for (benzene)₂ with an intermolecular separation of 3.95 Å, somewhat larger than the best-available estimate of 3.8 Å.⁶⁸ If anything, it seems likely that the effects of charge penetration are underestimated at the geometries used here for (corannulene)₂.
- (107) Kennedy, M. R.; Burns, L. A.; Sherrill, C. D. Buckyplates and buckybowl: Examining the effects of curvature on π - π interactions. *J. Phys. Chem. A* **2012**, *116*, 11920–11926.
- (108) Pérez, C.; Steber, A. L.; Rijs, A. M.; Temelso, B.; Shields, G. C.; Lopez, J. C.; Kisiel, Z.; Schnell, M. Corannulene and its complex with water: A tiny cup of water. *Phys. Chem. Chem. Phys.* **2017**, *19*, 14214–14223.
- (109) Hovick, J. W.; Poler, J. C. Misconceptions in sign conventions: Flipping the electric dipole moment. *J. Chem. Educ.* **2005**, *82*, 889.
- (110) Sharpe, A. G. The solvation of halide ions and its chemical significance. *J. Chem. Educ.* **1990**, *67*, 309–315.
- (111) Antalek, M.; Pace, E.; Hedman, B.; Hodgson, K. O.; Chillemi, G.; Benfatto, M.; Sarangi, R.; Frank, P. Solvation structure of the halides from x-ray absorption spectroscopy. *J. Chem. Phys.* **2016**, *145*, 044318.
- (112) Ayotte, P.; Weddle, G. H.; Kim, J.; Johnson, M. A. Vibrational spectroscopy of the ionic hydrogen bond: Fermi resonances and ion–molecule stretching frequencies in the binary $X^- \cdot H_2O$ ($X = Cl, Br, I$) complexes via argon predissociation spectroscopy. *J. Am. Chem. Soc.* **1998**, *120*, 12361–12362.
- (113) Robertson, W. H.; Johnson, M. A. Molecular aspects of halide ion hydration: The cluster approach. *Annu. Rev. Phys. Chem.* **2003**, *54*, 173–213.
- (114) Roscioli, J. R.; Diken, E. G.; Johnson, M. A.; Horvath, S.; McCoy, A. B. Prying apart a water molecule with anionic H-bonding: A comparative spectroscopic study of the $X^- \cdot H_2O$ ($X = OH, O, F, Cl, \text{ and } Br$) binary complexes in the 600–3800 cm^{-1} region. *J. Phys. Chem. A* **2006**, *110*, 4943–4952.
- (115) Xantheas, S. S. Quantitative description of hydrogen bonding in chloride–water clusters. *J. Phys. Chem.* **1996**, *100*, 9703–9713.
- (116) Baik, J.; Kim, J.; Majumdar, D.; Kim, K. S. Structures, energetics, and spectra of fluoride–water clusters $F^-(H_2O)_n$, $n = 1–6$: Ab initio study. *J. Chem. Phys.* **1999**, *110*, 9116–9127.
- (117) Combariza, J. E.; Kestner, N. R.; Jortner, J. Surface and interior states of iodide–water clusters. *Chem. Phys. Lett.* **1994**, *221*, 156–160.
- (118) Combariza, J. E.; Kestner, N. R.; Jortner, J. Energy-structure relationships for microscopic solvation of anions in water clusters. *J. Chem. Phys.* **1994**, *100*, 2851–2864.
- (119) Kim, J.; Lee, H. M.; Suh, S. B.; Majumdar, D.; Kim, K. S. Comparative ab initio study of the structures, energetics and spectra of

$X^-(\text{H}_2\text{O})_{n=1-4}$ [X = F, Cl, Br, I] clusters. *J. Chem. Phys.* **2000**, *113*, 5259–5272.

(120) Masamura, M. Structures, energetics, and spectra of $\text{Br}^-(\text{H}_2\text{O})_n$ clusters, $n = 1-6$: *Ab initio* study. *J. Chem. Phys.* **2003**, *118*, 6336–6347.

(121) Chamorro, Y.; Flórez, E.; Maldonado, A.; Aucar, G.; Restrepo, A. Microsolvation of heavy halides. *Int. J. Quantum Chem.* **2021**, *121*, e26571.

(122) Paul, S. K.; Herbert, J. M. Probing interfacial effects on ionization energies: The surprising banality of anion–water hydrogen bonding at the air/water interface. *J. Am. Chem. Soc.* **2021**, *143*, 10189–10202.

(123) Talbot, J. J.; Yang, N.; Huang, M.; Duong, C. H.; McCoy, A. B.; Steele, R. P.; Johnson, M. A. Spectroscopic signatures of mode-dependent tunnel splitting in the iodide–water binary complex. *J. Phys. Chem. A* **2020**, *124*, 2991–3001.

(124) Puranik, P. G.; Kumar, V. The charge transfer theory of the hydrogen bond. I. Theoretical. *Proc. - Indian Acad. Sci., Sect. A* **1963**, *58*, 29–37.

(125) Ratajczak, H.; Orville-Thomas, W. J. Charge transfer theory and vibrational properties of the hydrogen bond. *J. Mol. Struct.* **1973**, *19*, 237–245.

(126) Ratajczak, H. Charge-transfer properties of the hydrogen bond. I. Theory of the enhancement of dipole moment of hydrogen-bonded systems. *J. Phys. Chem.* **1972**, *76*, 3000–3004.

(127) Ratajczak, H. Charge-transfer properties of the hydrogen bond. II. Charge-transfer theory and the relation between the enhancement of dipole moment and the ionization potential of hydrogen-bonded systems. *J. Phys. Chem.* **1972**, *76*, 3991–3992.

(128) Ratajczak, H.; Orville-Thomas, W. J. Charge-transfer properties of hydrogen bonds. III. Charge-transfer theory and the relation between the energy and the enhancement of dipole moment of hydrogen-bonded complexes. *J. Chem. Phys.* **1973**, *58*, 911–919.

(129) Ratajczak, H.; Orville-Thomas, W. J.; Rao, C. N. R. Charge transfer theory of hydrogen bonds: Relations between vibrational spectra and energy of hydrogen bonds. *Chem. Phys.* **1976**, *17*, 197–216.

(130) Rao, C. N. R.; Dwivedi, P. C.; Ratajczak, H.; Orville-Thomas, W. J. Relation between O–H stretching frequency and hydrogen bond energy: Re-examination of the Badger-Bauer rule. *J. Chem. Soc., Faraday Trans. 2* **1975**, *71*, 955–966.

(131) Scheiner, S. *Hydrogen Bonding. A Theoretical Perspective*; Oxford University Press: New York, 1997.

(132) Weinhold, F.; Klein, R. A. What is a hydrogen bond? Mutually consistent theoretical and experimental criteria for characterizing H-bonding interactions. *Mol. Phys.* **2012**, *110*, 565–579.

(133) Ronca, E.; Belpassi, L.; Tarantelli, F. A quantitative view of charge transfer in the hydrogen bond: The water dimer case. *ChemPhysChem* **2014**, *15*, 2682–2687.

(134) Thompson, W. H.; Hynes, J. T. Frequency shifts in the hydrogen-bonded OH stretch in halide–water clusters. The importance of charge transfer. *J. Am. Chem. Soc.* **2000**, *122*, 6278–6286.

(135) Herbert, J. M.; Head-Gordon, M. Charge penetration and the origin of large O–H vibrational red-shifts in hydrated-electron clusters, $(\text{H}_2\text{O})_n^-$. *J. Am. Chem. Soc.* **2006**, *128*, 13932–13939.

(136) Ramos-Cordoba, E.; Lambrecht, D. S.; Head-Gordon, M. Charge-transfer and the hydrogen bond: Spectroscopic and structural implications from electronic structure calculations. *Faraday Discuss.* **2011**, *150*, 345–362.

(137) Kaduk, B.; Kowalczyk, T.; Van Voorhis, T. Constrained density functional theory. *Chem. Rev.* **2012**, *112*, 321–370.

(138) Stone, A. J. Natural bond orbitals and the nature of the hydrogen bond. *J. Phys. Chem. A* **2017**, *121*, 1531–1534.

(139) Bell, J. A. Getting it right: A paradigm for the education of chemists. In *Sputnik to Smartphones: A Half-Century of Chemistry Education*; American Chemical Society: Washington, DC, 2015; Vol. 1208, pp 25–43.

(140) Stone, A. J. Distributed multipole analysis: Stability for large basis sets. *J. Chem. Theory Comput.* **2005**, *1*, 1128–1132.

(141) Gordon, M. S.; Freitag, M. A.; Bandyopadhyay, P.; Jensen, J. H.; Kairys, V.; Stevens, W. J. The effective fragment potential method: A

QM-based MM approach to modeling environmental effects in chemistry. *J. Phys. Chem. A* **2001**, *105*, 293–307.

(142) Ghosh, D.; Kosenkov, D.; Vanovschi, V.; Williams, C. F.; Herbert, J. M.; Gordon, M. S.; Schmidt, M. W.; Slipchenko, L. V.; Krylov, A. I. Noncovalent interactions in extended systems described by the effective fragment potential method: Theory and application to nucleobase oligomers. *J. Phys. Chem. A* **2010**, *114*, 12739–12754.

(143) Ren, P.; Wu, C.; Ponder, J. W. Polarizable atomic multipole-based molecular mechanics for organic molecules. *J. Chem. Theory Comput.* **2011**, *7*, 3143–3161.

(144) Shi, Y.; Xia, Z.; Zhang, J.; Best, R.; Wu, C.; Ponder, J. W.; Ren, P. Polarizable atomic multipole-based AMOEBA force field for proteins. *J. Chem. Theory Comput.* **2013**, *9*, 4046–4063.

(145) Rackers, J. A.; Wang, Z.; Lu, C.; Lairy, M. L.; Lagardère, L.; Schnieders, M. J.; Piquemal, J.-P.; Ren, P.; Ponder, J. W. Tinker 8: Software tools for molecular design. *J. Chem. Theory Comput.* **2018**, *14*, 5273–5289.

(146) Wang, Q.; Rackers, J. A.; He, C.; Qi, R.; Narth, C.; Lagardère, L.; Gresh, N.; Ponder, J. W.; Piquemal, J.-P.; Ren, P. General model for treating short-range electrostatic penetration in a molecular mechanics force field. *J. Chem. Theory Comput.* **2015**, *11*, 2609–2618.

(147) Deng, S.; Wang, Q.; Ren, P. Estimating and modeling charge transfer from the SAPT induction energy. *J. Comput. Chem.* **2017**, *38*, 2222–2231.

(148) Schriber, J. B.; Nascimento, D. R.; Koutsoukas, A.; Spronk, S. A.; Cheney, D. L.; Sherrill, C. D. CLIFF: A component-based, machine-learned, intermolecular force field. *J. Chem. Phys.* **2021**, *154*, 184110.

(149) McDaniel, J. G.; Schmidt, J. R. Physically-motivated force fields from symmetry-adapted perturbation theory. *J. Phys. Chem. A* **2013**, *117*, 2053–2066.

(150) Schmidt, J. R.; Yu, K.; McDaniel, J. G. Transferable next-generation force fields from simple liquids to complex materials. *Acc. Chem. Res.* **2015**, *48*, 548–556.

(151) Slipchenko, L. V.; Gurunathan, P. K. Effective fragment potential method: Past, present, and future. In *Fragmentation: Toward Accurate Calculations on Complex Molecular Systems*; Gordon, M. S., Ed.; Wiley: Hoboken, NJ, 2017; pp 183–208.

(152) Jing, Z.; Liu, C.; Cheng, S. Y.; Qi, R.; Walker, B. D.; Piquemal, J.-P.; Ren, P. Polarizable force fields for biomolecular simulations: Recent advances and applications. *Annu. Rev. Biophys.* **2019**, *48*, 371–394.